Determining the Space and Density of Asphalt with the Help of a Non-Destructive Method Using a GPR Device and Modeling Their Relationship with Pavement Failures

Salar Sadeghi Nejad

Master in Civil Engineering, Construction Management
Islamic Azad University, Kerman Branch, Iran

Abstract- **Density is one of the criteria for measuring the quality of a road surface. The main goal of this research is to determine the void space and density of asphalt using a non-destructive method. In this research, a technical comparison was made regarding the accuracy of each method by using field observations by the GPR device and performing the necessary tests on the samples obtained from coring. Then Marshall's indirect tensile stress test was performed to measure the percentage of free space of experimental stone materials known as the Raice test. Finally, with the help of MATLAB normalization, our communication model between the test results was presented. Finally, it was found that there is a significant relationship between the actual density of the asphalt and the constant coefficient of the dielectric, that the relationship between these two is linear, and if the percentage of extra space increases, the dielectric will decrease. In addition, in the case of comparing the recognition, the amount of stripping with the qualitative interpretation of the results obtained by taking the profiles with the device reached 78.5% with 22.5% error.**

***Keywords*: Pavement failures; Asphalt density; Dielectric coefficient; Tensile stress test.**

RESUMEN
La densidad es uno de los criterios para medir la calidad de la superficie de una carretera. El objetivo principal de esta investigación es determinar el espacio vacío y la densidad del asfalto utilizando un método no destructivo. En esta investigación se realizó una comparación técnica en cuanto a la precisión de cada método utilizando observaciones de campo por el dispositivo GPR y realizando las pruebas necesarias en las muestras obtenidas de la extracción de testigos. Luego se realizó la prueba de esfuerzo de tracción indirecta de Marshall para medir el porcentaje de espacio libre de los materiales pétreos experimentales conocida como prueba Raice. Finalmente, con la ayuda de la normalización de MATLAB, se presentó nuestro modelo de comunicación entre los resultados de las pruebas. Finalmente, se encontró que existe una relación significativa entre la densidad real del asfalto y el coeficiente constante del dieléctrico, que la relación entre estos dos es lineal, y si aumenta el porcentaje de espacio vacío extra, el dieléctrico disminuirá. Además, en el caso de comparar el reconocimiento, la cantidad de decapado con la interpretación cualitativa de los resultados obtenidos al tomar los perfiles con el dispositivo alcanzó el 78.5% con un 22.5% de error.

Palabras claves: Fallas en el pavimento; Densidad del asfalto; Coeficiente dieléctrico; Ensayo de tensión de tracció

1. INTRODUCTION

Density is an important component in the design and implementation of asphalt pavement. It is very important to choose the appropriate level of compaction in the mixing design stage for the proper performance of the pavement. Density is one of the most important parameters in the asphalt mixture structure (Aschenbrener et al., 2020; Diamanti et al., 2021). A mixture with a proper mixing and compaction plan includes a sufficient percentage of free space to prevent the occurrence of creasing due to plastic flow and also a low percentage of free space to prevent water and air penetration (Duarte & Faxina, 2021).

Correct measurement of density at a hot asphalt mix site is essential for quality control and assurance, performance prediction, and contractor control (Meghna & Puppanna, 2018; Wang et al., 2022a). Right now, the most common method to determine the density of asphalt mixture in the country is the coring method (Fakhri & Shahni Dezfoulian, 2019). The test of measuring the density by the nuclear method is usually used in research and academic projects. Coring is a proven method for determining the density and is considered the most reliable and accurate method of determining density, But this method is destructive (holes resulting from coring must be patched and repaired) and it is also difficult and time-consuming. Perhaps the most negative aspect of coring is the long time spent determining the density on the spot. The cores must first be transported to the laboratory. It may be a considerable distance between the location of the road construction operation and the laboratory (Leng et al., 2018). This process may take from a few hours to a day depending on the project status. Regardless of the operation time, if the contractor is not sure about the density at the site, coring must continue (Joshaghani & Shokrabadi, 2022). Asphalt concrete density is divided into two types: Bulk specific gravity (Gmb) and maximum specific gravity (Gmm) (Yan, 2012). According to AASHTO standard T166 (Association American of State Highways and Transportation Officials standards, 2008), the actual density is obtained by weighing cored samples after spreading and compacting paraffin-coated asphalt in water and air.

The importance of asphalt density calculation and also the need to introduce an accurate method that can provide a continuous profile of asphalt density along the axis at high speed shows why this is the case. Introducing the ground penetrating radar method, which is one of the newest technologies in the world in the field of engineering sciences, as a method that meets the above requirements and provides useful information on the way, can be very helpful (Ghanim, 2022). Also, density is an important component in the design and implementation of asphalt pavement. It is very important to choose the appropriate level of compaction in the mixing design stage for the proper performance of the pavement (Fernandes et al., 2017). Density is one of the most important parameters in the asphalt mixture structure. A mixture with a proper mixing and compaction plan includes a sufficient percentage of space to prevent the occurrence of creasing due to plastic flow and also a low percentage of space to prevent water and air penetration (Fernandes et al., 2017; Sreedhar & Coleri, 2018). Considering that the density of the asphalt mixture changes during its lifetime, the percentage of space should be small enough to prevent air and water penetration and also high enough to prevent plastic flow in the asphalt mixture after passing traffic after some years have passed (Brown, 1990; Yan, 2012); Therefore, the correct measurement of the density at the site of hot asphalt mixture is necessary to control and guarantee the quality, predict the performance, and control the contractor.

In this research, the density of asphalt was determined using electromagnetic methods, which is one of the non-destructive methods (Wang et al., 2022b). The GPR (Ground Penetrating Radar) method is one of the newest electromagnetic methods that found wide applications in engineering sciences, especially road construction (Rhee et al., 2020). Many studies have been conducted in the field of investigation and expansion of these applications in prestigious institutions and universities of the world (Cui et al., 2021; Kassem et al., 2016; Teshale et al., 2020; Wang et al., 2018, 2019, 2020), which have had very good results.

Among these applications, we can mention the calculation of density with this method, which is one of the latest topics raised about this technology. By sending and receiving electromagnetic waves and calculating their return speed, the GPR device calculates the dielectric of the pavement layers and provides useful information such as the thickness of the layers, the asphalt density, the amount of moisture content, the characteristics of the buried facilities, etc.

2. MATERIALS AND METHODS

2.1 Research method

The general purpose of this research is to evaluate the ability to use the ground penetrating radar device (ground penetrating radar) in detecting the density in asphalt mixtures. and performing other destructive tests, a technical comparison between these 2 methods should be made in understanding the problem, finally, the results obtained from the tests and the relationships used in the ground penetrating radar method should be calibrated for use in Iran. The method used in this research is both a survey type and an experimental type. For the survey type, 2 axes of Amir Kabir Boulevard from east to west and vice versa from Nakhl Boulevard from north to south have been used. After surveying with a ground penetrating radar device, from the same axes, with taking and conducting destructive tests, in this study, a laboratory method is used to conduct the research. One of the basic characteristics of this research method is the use of a control sample (control). In other words, the selection of the control group shows one of the foundations of the research method. The framework of this method is very simple. In this research method, the analysis of the results obtained from the survey of the studied route is compared with the sampling of the same axis and destructive tests in the laboratory. In this method, finally, laboratory results for density detection should give similar results to the results of surveying with the device, ground penetrating radar, and in similar conditions. In this case, the findings of the research were generally used.

2.2 Selection of the Studied Axis

According to the investigations carried out on the road network of the 22nd district of Tehran due to the arterial nature of Amir Kabir Boulevard and the maximum volume of passing traffic, due to the connection of the Azadegan highway to the Chitgar region and west of Tehran from it, the amount of damage observed on the surface was more severe. The pavement was observed compared to other roads and roads compared to other streets in the region, so one of the selected routes is the return route of Amir Kabir Boulevard from the east to the west between Azadegan Highway in the east to Kashan Boulevard (leading to Chitgar Lake) in the west and vice versa. Figure (1) and Table (1) (showing the characteristics of the route and its length) also show satellite images from the beginning and the end of one of the axes of the survey (Amir Kabir Boulevard) and also by evaluating the road network of the 2nd region of Tehran, the north-south route Nakhl Street, between Mahalati Square and Army Highway, was chosen as the second axis (survey-laboratory) due to the variety of climate, cold temperature, and temperature difference compared to the first survey.

Figure 1. Map of the location of the first survey (Amirkabir Boulevard, Tehran, Iran)

Table 1 - Specifications of the evaluated axis in Amirkabir Blvd

Axis length	end path coordinates	start path coordinates	Axis specifications	Axis name
2350 m	X=51228847 Y=35746160	X=51253967 Y=35748820	has 3 crossing lanes of the main arterial grade 1 boulevard	East to West Amir Kabir
2350 m	X=5125393 Y=35747992	X=51228847 Y=35746160	has 3 crossing lanes of the main arterial grade 1 boulevard	West to East Amir Kabir

Figure (2) and Table (2) (showing the characteristics of the route and its length) also show satellite images from the beginning and end of one of the survey axes (Nakhl Street).

Figure 2. Map of the second survey (Nakhl Street, Tehran, Iran)

Table 2- Characteristics of the assessed axis in Amirkabir Blvd

Axis length	end path coordinates	start path coordinates	Axis specifications	Axis name
840 m	X=51508687 Y=35799275	X=51508687 Y=35799275	Has 2 lanes 1st-grade main road	North to South Nakhl

2.3 Collection of data and information

By inquiring from the meteorological and municipal organization, the temperature and construction history of regions 2 and 22 are shown according to the specifications of the table (3-4).

Table 3. Temperature specifications and manufacturing history

Construction history	The temperature on surveying time	Axis specifications
Covered twice in 2007 and 2009	20 degrees Celsius	Amirkabir Blvd
Covered once in 2011	17 degrees Celsius	Nakhl Blvd

2.4 Selecting the coring location and determining the damage percentage by the visual survey of pavement Surface

After determining the evaluation axes and carrying out the mechanized survey, based on the visual inspection of the pavement surface and assigning the percentage of damage to it, in some places along the route, in all 2 axes, sampling is done at the specified points. Figure (3) shows the damage to the pavement surface is high and low, respectively, from right to left.

Figure 3. damage to the pavement surface

2.5 Coring Operation

After determining the coring location from the specified locations, the coring operation is carried out. The important point during the coring operation is that due to the increased friction of the machine's drill wall with the road surface, during the coring operation, there is a possibility of the core getting stuck in the asphalt or the electric motor burning due to excessive pressure, so to avoid this problem (reducing the friction of the wall of the drill with asphalt and cooling of the drill) during coring, water must be pumped into the drill through the tank connected to it, in case of a sudden change in sound during drilling and cutting, the drill must be raised immediately by the hand lever connected to the hydraulic jack of the drill Because the change in sound indicates the change of the asphalt layer and the drill reaching the roadbed or subgrade. Finally, after the machine is turned aside, the core is removed by special pliers.

2.6 Visual Survey of the Cores

Before the beginning of the visual survey stage, the location of coring in all 2 axes should be determined, then 2 cores were taken from each axis with the coring device, and after that, the depth of damage was estimated visually by visual inspection and with The healthy core (control) should be compared. Figure (4) shows samples taken from the core at 2230 km from the west to east of Amir Kabir Blvd.

Figure 4. A Sample of the core

2.7 Preparing the core for the laboratory method

First, each of the 2 cores extracted from each axis is cut to a thickness of 5 cm. Figure (5) shows how the cores are cut into 5 cm pieces. Then, after cutting each of the cores, a numbering is done on each of them, in a way that each core is compared 2 by 2 for evaluation (Figure 6).

Figure 5. Cutting the cores

Figure 6. Preparing the cores in 2 saturated and dry states

2.8 Performing Mechanical Tests

After the survey is carried out in the assessed routes, it is time to conduct destructive tests, the results of each test are compared with the values obtained from the interpretation of the ground penetrating radar.

Density determination test: According to the division of the cores taken, the method of performing this test is that the sample is first weighed in the air and recorded. Then the weight of the same sample immersed in water is also recorded. From the difference between these two states, i.e. the weight of the sample in water and air, the actual specific gravity of asphalt is obtained. The test method is given in ASTM standard 1188. Equation (2) is used to determine the density.

$$G_{mb} = \frac{W_a}{W_a - W_w} \qquad (2)$$

In which, Wa is the weight of samples in air, Ww is the weight of samples in water, and Gmb is the actual specific gravity of asphalt. Figure (7) shows the weighing of asphalt samples in air and water.

Figure 7. Weighing asphalt samples in air and water

The test to determine the free space: After performing the Marshall indirect tensile stress test, to measure the percentage of free space of stone materials, a test known as the Raice test is performed. In this test, the empty spaces of 2 corresponding samples are compared. In this test, the samples removed from the Marshall devices are placed in the greenhouse to open well. Then, by dividing it into four parts, about 120 grams of the mixture is selected and poured into the Erlenmeyer flask, whose dry and water-filled weight is obtained. Next, about one-third of the volume of the Erlenmeyer flask containing the asphalt sample is filled with water and after closing the lid, The vacuum device is connected to remove the air between the asphalt particles.

Finally, after removing all the air between the particles of the mixture, the flask is separated from the device and filled with water up to the marked line, and its weight is measured. The test method is given in ASTM standard 2041. Now, with the help of equations (3) and (4), the percentage of space in the asphalt mixture can be measured:

$$G_{mm} = \frac{A}{A + D - E} \qquad (3)$$

$$A.V = 100 \times \left(1 - \frac{G_{mb}}{G_{mm}}\right) \quad (4)$$

in which, G is the maximum specific millimeter weight,
A is the weight of the dry sample in the air (grams) (about 120 grams),
D is the weight of the Erlenmeyer filled with water (grams),
and E is the weight of the Erlenmeyer containing the asphalt sample and filled with water (grams),
A.V. is the percentage of space of asphalt mixture and
Gmb is the actual density of asphalt concrete obtained from equation (2).
Raise test equipment can be seen in Figure (8).

Figure 8. Raise test equipment

3. RESULTS AND DISCUSSION

3.1 Extracting the Results

The results obtained from the mechanized survey and mechanical destructive tests are entered in Microsoft Office - Excel software and we compare the graphs that show the visual survey, the percentage of space, and the specific weight of asphalt samples with the output results of the ground penetrating radar device. Finally, with the help of MATLAB software, the communication model between the results is presented.

3.2 Breakdown and analysis of the results

After determining the evaluation axes and carrying out the mechanized survey, based on the visual inspection of the pavement surface and assigning the percentage of damage (such as exposure and weathering) to it, in some places along the route, in every 2 axes, cores are taken at the specified points. Figure (9) shows the damage to the pavement surface is high and low from right to left, respectively.

Figure 9. Damage to the pavement Surface

Each of these points has been named and visually inspected, its percentage of failure has been determined, and its results are verified by qualitative interpretation.
Table (4) shows the specifications of the routes that were used for visual evaluation.

Table 4. Specifications of evaluated routes

Point number	A	B	C	D	E	F	G	H
Point specifications	W-E – 0+150 km	W-E – 0+750 km	W-E – 1+870 km	W-E – 2+230 km	E-W – 0+320 km	E-W – 2+020 km	N-S – 0+315 km	N-S – 0+715 km

The next step after applying appropriate processing to the data is the interpretation of radar profiles. This method of interpretation, which is also known as graphic interpretation, is done by using prominent features on the radar sections. In this way, the obtained time sections may be converted into depth sections in the subsurface environment using the speed of radar waves, or they may be interpreted directly. In this type of interpretation, the analyzer recognizes the quality and shape of the reflections compared to the adjacent reflections and separates these events from each other according to the characteristics of these reflections, including their continuity, magnitude, and expansion.

As shown in Figure 10 of the initial 150-meter profile of the west to the east route of Amir Kabir Boulevard, along with the graphic output and the peak value of the domain, the shape of the diagram is almost uniform in the first layer and no particular damage is observed. The value of the approximation range is 6400.2 millivolts1 (with a reflection time of 3.6 nanoseconds). Figure 11 is also an example of the profile taken in the 715-meter area of the north-south route of Nakhl. In the observed pavement, especially in the area of 715 meters, abnormal amplitudes can be seen. Meanwhile, the numerical value of the amplitude is 225.1 millivolts (about 3.71 reflection time in terms of nanoseconds) and the marginal decrease of the amplitude also confirms the cause of the damage and the presence of air in the mentioned section.

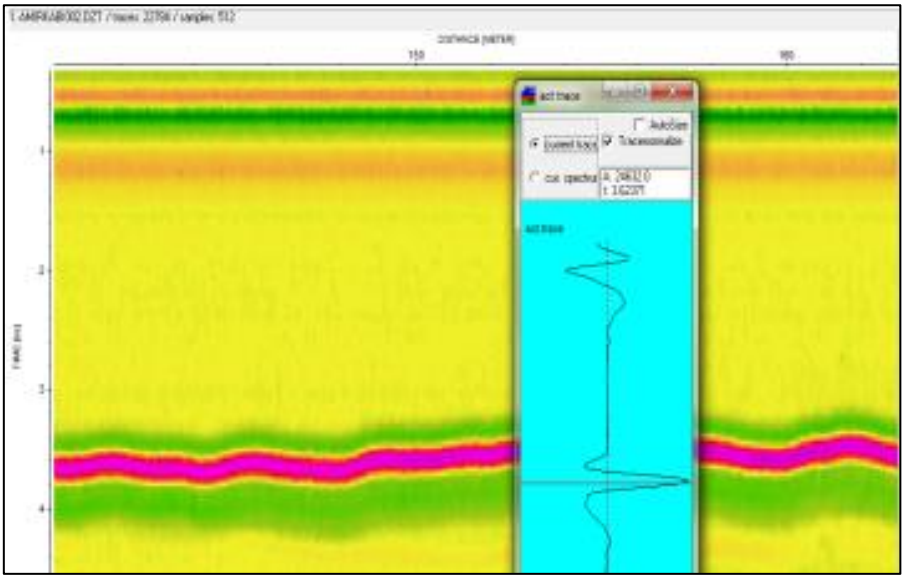

Figure 10. Profile taken with the mechanized device, Amirkabir axis

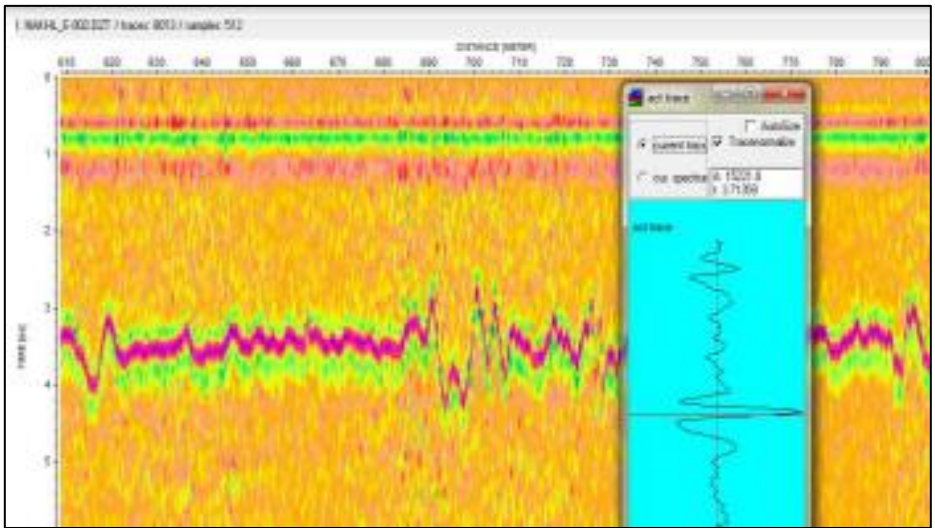

Figure 11. Profile taken with the mechanized device, Nakhl axis

[1] - For calculation simplicity, all the output numbers of domains are divided by 10000 in this research

In short, by qualitatively examining the radar output profiles and interpreting the failures, it is possible to estimate the depth of the asphalt layers in the evaluated routes, as well as the depth of the failure with this method, which shows the summary of the qualitative interpretation of the collected profiles in Table (5).

Table 5. Summary of the qualitative interpretation of the collected profile

Point number	**A**	**B**	**C**	**D**	**E**	**F**	**G**	**H**
Point specifications	W-E – 0+150 km	W-E – 0+750 km	W-E – 1+870 km	W-E – 2+230 km	E-W – 0+320 km	E-W – 2+020 km	N-S – 0+315 km	N-S – 0+715 km
Evaluation date	October 2nd, 2015	October 2nd, 2015	October 2nd, 2015	October 2nd, 2015	October 2nd, 2015	October 2nd, 2015	October 2nd, 2015	October 2nd, 2015
Qualitative observations	Stripped	Not stripped	Not stripped	Not stripped	Not stripped	Not stripped	Not stripped	Stripped

3.3 The results of the visual survey of the pavement Surface

Based on the visual inspection of the pavement surface and assigning the percentage of damage to it, the surface is evaluated visually in some places of the route before the coring operation. Figures (12) to (19) show pictures taken from the pavement surface under evaluation.

Figure 12. Pavement surface in A

Figure 13. Pavement surface in B

Figure 14. Pavement surface in C

Figure 15. Pavement surface in D

Figure 16. Pavement surface in E

Figure 17. Pavement surface in F

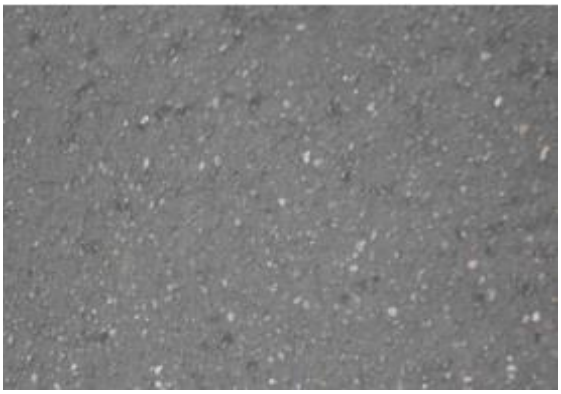

Figure 18. Pavement surface in G

Figure 19. Pavement surface in H

Like the PCI method, each of the images is given a percentage of failure numerically; The summary results of this eye survey are shown in table (6).

Table 6. Results of the visual survey of pavement Surface

Point number	**A**	**B**	**C**	**D**	**E**	**F**	**G**	**H**
Point specifications	W-E – 0+150 km	W-E – 0+750 km	W-E – 1+870 km	W-E – 2+230 km	E-W – 0+320 km	E-W – 2+020 km	N-S – 0+315 km	N-S – 0+715 km
coring date	November 9th 2015	November 9th 2015	November 9th 2015	November 9th 2015	November 9th 2015	November 9th 2015	October 12th 2015	October 12th 2015
Failure percentage	25	70	60	30	45	20	30	100

3.4 Visual survey of cores

After coring, the depth of the suspected damage in the core is determined by the observation method. Figures (20) and (21) are examples of observations of cores of the path 750 meters north to south of Nakhl and 320 meters east to west of Amir Kabir Boulevard, respectively.

Figure 20. The core of the north-south route of Nakhl Street

Figure 21. The core of the east-west route of Amirkabir Blvd

3.5 Performing mechanical tests

To validate the accuracy of the ground penetrating radar data, the values taken and interpreted by the device are first compared with visual observations, then compared with the results of mechanical destructive tests at the points of the axis where the core is taken.

3.6 Preparation of the core to perform mechanical tests

To perform mechanical tests, the cores must be cut and used, for this purpose, 2 cores are taken from each point, and the upper surfaces of each of the cut samples are compared with each other in the dry and saturated state. (Dry state: After cutting, the samples are kept for 2 hours at a temperature of 25 degrees Celsius in an immersed container so that 7 cm of water is covered above it, and then they are used. Saturated state: the samples are kept at 60 degrees for 24 hours and after coming out of the hot water bath, they are kept at 25 degrees for 2 hours after adjusting to the ambient temperature). Another reason for cutting and comparing 2 dry and saturated states at the same depth is that at each depth, the specifications of asphalt pavement, including the grading, layer material, and density of each layer are different.

3.7 Numbering of simples

To identify the upper levels of each core and to identify the 2 cores taken from the same path, the relevant tests and 2 by 2 comparison of each of the samples are done by numbering. Therefore, each sample is numbered by color. Table (7) shows the specifications of the cores and the numbers assigned to each one.

Table 7. numbering of simple

Dry sample	**1**	**First 5 cm**	**second 5 cm**	**third 5 cm**	**fourth 5 cm**
Wet sample	1				
West to east Amir Kabir	First core	1	3		
150 km	Second core	2	4		
West to east Amir Kabir	First core	5	7	9	11
750 km	Second core	6	8	10	12
West to east Amir Kabir	First core	13	15	17	19
1870 km	Second core	14	16	18	20
West to east Amir Kabir	First core	21	23		
2230 km	Second core	22	24		
East to west Amir Kabir	First core	25	27	29	
320 km	Second core	26	28	30	
East to west Amir Kabir	First core	31	33	35	
2020 km	Second core	32	34	36	
North to south Nakhl	First core	37	39	41	
315 km	Second core	38	40	42	
North to south Nakhl	First core	43	45	47	49
715 km	Second core	44	46	48	50

3.8 Density determination test

According to the division of cores in the first layer (first 5 cm), the density values are shown in table (8) (actual density (Gmb), (Gmm) is the maximum density)

Table 8. The density of cores in the dry and saturated state

Mileage number	**0+715**	**0+315**	**2+020**	**0+320**	**2+230**	**1+870**	**0+750**	**0+150**

Gmb g/cm²	2.1635	2.2085	2.2995	2.1865	2.16	2.1705	2.1395	2.199
dielectric	4.91	6.25	5.76	4.94	4.91	4.87	4.94	5.09
Gmm	2.41	2.32	2.38	2.4	2.4	2.4	2.43	2.41
Core number	8	7	6	5	4	3	2	1

3.9 Test to determine space

According to the categorization of cores, in the first layer (5 cm) the values of free space are shown in table (9). The relationship between the percentages of space in mileage is shown in the diagram in figure (22).

Table 9. percentage of space of cores

Core mileage	**0+715**	**0+315**	**2+020**	**0+320**	**2+230**	**1+870**	**0+750**	**0+150**
core number	8	7	6	5	4	3	2	1
Percentage of space	10.22	4.86	3.38	8.89	10	9.56	11.95	8.75
Dielectric	4.91	6.25	5.47	4.94	4.91	4.87	4.90	5.09

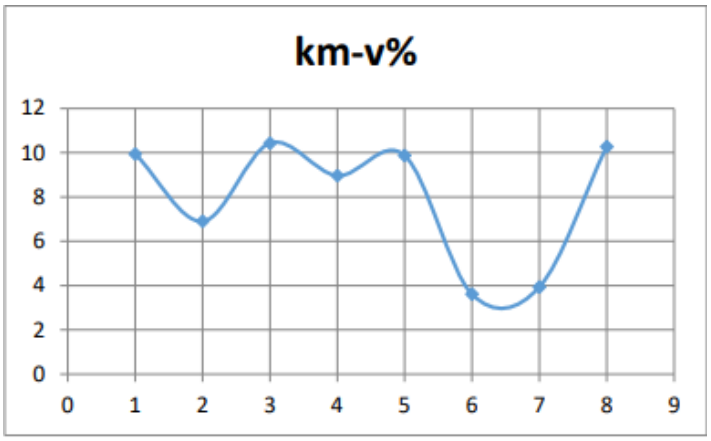

Figure 22. Graph of the percentage of space of cores in different mileage

3.10 Analysis of results

3.10.1 The relationship between the visual evaluation of cores and TSR

As seen in Table 10, TSR values that are less than 2.7 (according to the T283 standard) are stripped cores to moisture. By comparing the visual method and the test of indirect tensile stress ratio (TSR) in 7 samples from the upper surface of the taken cores, the percentage of accuracy of detecting the denudation hypothesis in this method was 85%.

Table 10. Comparing the visual method with TSR

core number	**1 2**	**5 6**	**13 14**	**21 22**	**25 26**	**31 32**	**37 38**	**41 42**
TSR	0.75	0.8	0.93	1.15	0.68	0.88	0.48	0.71
evaluation based on the TSR index	0.75<0.8 Low stripping	0.8≥0.8 Limit of healthy stripping	0.8<0.93 Not stripped healthy	0.8<1.15 Not stripped healthy	0.68<0.8 stripped	0.88≥0.9 Limit of healthy stripping	0.48<0.8 Extreme stripping	0.71<0.8 Stripped
evaluation based on visual observation	Not stripped	Not stripped	Not stripped	Not stripped	Not stripped	Not stripped	Not stripped	Stripped
Verification of visual survey with TSR	Incorrect	Correct	Correct	Correct	Correct	Correct	Incorrect	Correct
Results	Total number of cores=8, percentage of error=25%, percentage of visual method's accuracy= 75%							

The relationship between mechanized qualitative interpretation and TSR: As seen in table (11), TSR values that are less than 2.7 are stripped cores in humidity according to the T283 standard. By comparing the mechanized qualitative interpretation and testing the indirect tensile stress ratio (TSR) in 7 samples from the upper surface of the taken cores, the accuracy percentage of the hypothesis of stripping detection with this method was 78.5%.

Table 11. Comparing the mechanized qualitative interpretation method with TSR

core number	1 2	5 6	13 14	21 22	25 26	31 32	37 38	41 42
TSR	0.75	0.8	0.93	1.15	0.68	0.88	0.48	0.71
evaluation based on the TSR index	0.75<0.8 Low stripping	0.8≥0.8 Limit of healthy stripping	0.8<0.93 Not stripped healthy	0.8<1.15 Not stripped healthy	0.68<0.8 stripped	0.88≥0.9 Limit of healthy stripping	0.48<0.8 Extreme stripping	0.71<0.8 Stripped
evaluation based on mechanized qualitative interpretation	Stripped	Not stripped	Not stripped	Not stripped	Not stripped	Not stripped	Not stripped	Stripped
Verification of visual survey with TSR	Correct	Correct	Correct	Correct	Incorrect	Correct	Correct	Correct
Results	Total number of cores=8, percentage of error=5.12%, percentage of mechanized qualitative interpretation's accuracy= 75%							

The relationship between density and radar's qualitative interpretation: According to table (12), the density values are compared with each other with the interpretation resulting from the analysis of the data of the ground penetrating radar device.

Table 12. Comparing density with radar interpretation

Mileage number	0+715	0+315	2+020	0+320	2+230	1+870	0+750	0+150
Gmb	2.1635	2.2085	2.2995	2.1865	2.16	2.1705	2.1395	2.199
Dielectric	4.98	6.25	5.76	4.94	4.91	4.87	4.94	5.09
Gmm	2.41	2.32	2.38	2.4	2.4	2.4	2.43	2.41
Core number	8	7	6	5	4	3	2	1
Evaluation based on mechanized qualitative interpretation	failure	healthy	healthy	healthy	healthy	healthy	healthy	failure

According to the results of the qualitative interpretation of the radar data with the dielectric constant obtained from the output of the amplitudes caused by the radar device. Where the dielectric coefficient has the highest values, the cores are damaged, and when we obtain the relationship between the dielectric coefficient and the maximum density of asphalt, it can be seen that this relationship is linear with a correlation coefficient of 0.8 (Figure 23).

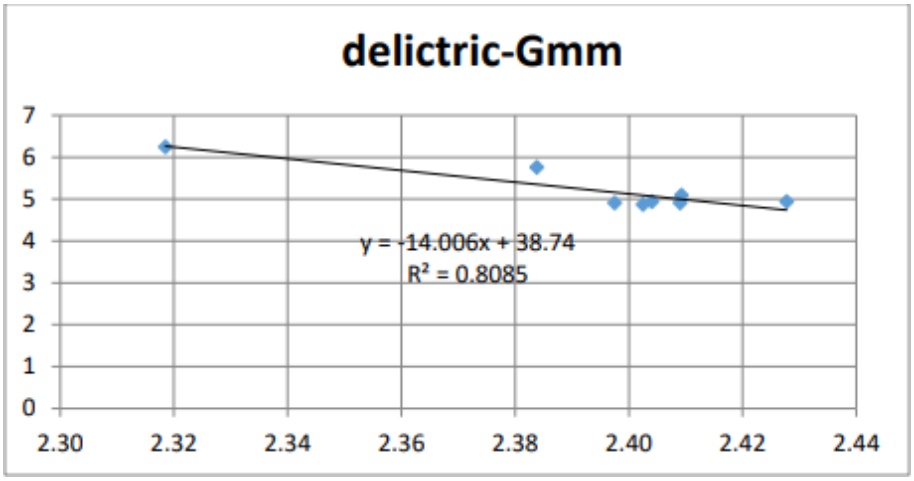

Figure 23. Dielectric coefficient diagram with maximum density

The relationship between the percentage of space and the dielectric coefficient: The ratio of free space resulting from the Raice test and the dielectric coefficient is inversely proportional to each other, As shown in table (13). In the values that show the largest number in percent of space, the dielectric coefficient also shows the lowest value in the highest percentage of free space. Figure (24) shows the ratio of the percentage of space to the dielectric constant, which is an exponential function with a correlation

coefficient of 0.81. By using the standard method of conducting this test (ASTM 2041)2, according to the standard, to achieve a higher correlation, outlier data, if any, are corrected or removed.

Table 13. Percentage of space of cores

Mileage number	**0+715**	**0+315**	**2+020**	**0+320**	**2+230**	**1+870**	**0+750**	**0+150**
Core number	8	7	6	5	4	3	2	1
Percentage of space	10.22	4.86	3.38	8.89	10	9.56	11.95	8.75
Evaluation based on mechanized qualitative interpretation	failure	healthy	healthy	healthy	healthy	healthy	healthy	failure

As seen in the values of Table 13, the samples that are damaged have the most extra space, and the relationship between the percentage of space and the dielectric constant is an exponential function according to Figure 24.

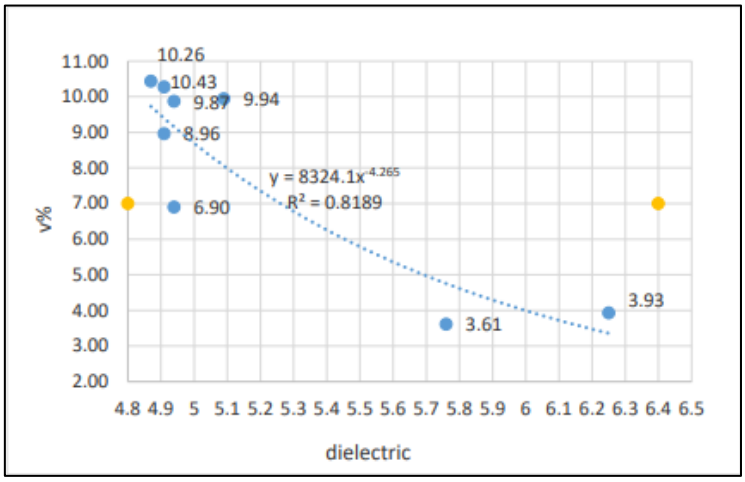

Figure 24. The diagram of the relationship between the dielectric coefficient and the percentage of space

The relationship between indirect tensile stress (TSR) and dielectric coefficient: The ratio of indirect tensile stress is one of the important factors for determining to strip. The values of a table (14) show that if there is stripping, the amount of indirect tensile load in the saturated state shows a greater decrease compared to the load in the dry state. The lower the breaking threshold load of the core in the saturated state compared to the dry, the more intense moisture damage the core has. The saturated-to-dry load ratio of 2.7 refers to the limit of stripping, the smaller values of the weak and stripped sections, and the samples with values of this ratio of 2.7 and above are acceptable and resistant to stripping and damage caused by moisture.

Table 14. Indirect tensile stress in the saturated and dry state, dielectric coefficient

core number	**1 2**	**5 6**	**13 14**	**21 22**	**25 26**	**31 32**
TSR	0.75	0.8	0.93	1.15	0.68	0.88
evaluation based on the TSR index	0.75<0.8 Low stripping	0.8≥0.8 Limit of healthy stripping	0.8<0.93 Not stripped healthy	0.8<1.15 Not stripped healthy	0.68<0.8 stripped	0.88≥0.9 Limit of healthy stripping
Saturated indirect tensile stress	6.087	6.191	7.164	7.688	4.78	4.505
dry indirect tensile stress	8.15	7.782	7.667	6.667	7.071	9.379
Irnli	14.26	10.55	10.82	17.02	14.26	7.19

4. CONCLUSION

According to the results, the relationship between accuracy in recognition of stripping (one of the types of failure) in the visual survey method with a TSR ratio of 25% error was verified with 85% accuracy. In addition, comparing recognition of tripping with the qualitative interpretation of the results obtained by taking the profiles with the device (mechanized survey), with an error of 22.5%, reaching 78.5%. According to the tests of the maximum density of asphalt and the percentage of space (resulting from the Raice test) and Its relationship with the dielectric constant taken from the radar output results, it can be concluded that there is a

[2] - Standard Test Method for Theoretical Maximum Specific Gravity and Density of Bituminous Paving Mixtures

significant relationship between the actual density of asphalt and the dielectric constant coefficient, and the relationship between the two is linear. Also, if there is more free space in percent, the dielectric value will decrease. The diagram of the relationship between dielectric and free space is a relation of an exponential function. Considering that extra free space is an important factor in the occurrence of exposure and traffic has a direct conflict with exposure, the evaluation of each axis, and the amount of traffic at the selected crossings and axes are preferably selected among the areas with heavy traffic and if there are facilities for testing, the non-destructive device UTM 25 can also be used to model the traffic load and temperature.

REFERENCES:

1. Aschenbrener, T., Brown, E. R., Tran, N. H., Blankenship, P. B., & Technology, A. University. N. C. for A. *Demonstration Project for Enhanced Durability of Asphalt Pavements through Increased In-Place Pavement Density*. (2020). https://doi.org/10.21949/1503647
2. Association American of State Highways and Transportation Officials standards. AASHTO standards. *Part 2A Tests, Twenty Eight*, 1059. (2008).
3. Brown, E. R. Density of Asphalt Concrete - How Much is Needed? *Transp. Res. Rec.*, *1282*(1), 27–32. (1990). https://doi.org/10.21949/1404494
4. Cui, L., Ling, T., Zhang, Z., Xin, J., & Li, R. Development of asphalt mixture density estimation model applicable to wide air void content range using ground penetrating radar. *Construction and Building Materials*, *293*, 123521. (2021). https://doi.org/10.1016/J.CONBUILDMAT.2021.123521
5. Diamanti, N., Annan, A. P., Jackson, S. R., & Klazinga, D. A GPR-Based Pavement Density Profiler: Operating Principles and Applications. *Remote Sensing*, *13*(13), 2613. (2021). https://doi.org/10.3390/rs13132613
6. Duarte, G. M., & Faxina, A. L. Asphalt concrete mixtures modified with polymeric waste by the wet and dry processes: A literature review. *Construction and Building Materials*, *312*, 125408. (2021). https://doi.org/10.1016/J.CONBUILDMAT.2021.125408
7. Fakhri, M., & Shahni Dezfoulian, R. Pavement structural evaluation based on roughness and surface distress survey using neural network model. *Construction and Building Materials*, *204*, 768–780. (2019). https://doi.org/10.1016/J.CONBUILDMAT.2019.01.142
8. Fernandes, F. M., Fernandes, A., & Pais, J Assessment of the density and moisture content of asphalt mixtures of road pavements. *Construction and Building Materials*, *154*, 1216–1225. . (2017). https://doi.org/10.1016/J.CONBUILDMAT.2017.06.119
9. Ghanim, N. K. G. *GPR as an alternative method for measuring asphalt pavement density* [BACHELOR THESIS]. The University of Twente. (2022).
10. Joshaghani, A., & Shokrabadi, M. Ground penetrating radar (GPR) applications in concrete pavements. *International Journal of Pavement Engineering*, *23*(13), 4504–4531. (2022). https://doi.org/10.1080/10298436.2021.1954182
11. Kassem, E., Chowdhury, A., Scullion, T., & Masad, E. Application of ground-penetrating radar in measuring the density of asphalt pavements and its relationship to mechanical properties. *International Journal of Pavement Engineering*, *17*(6), 503–516. (2016). https://doi.org/10.1080/10298436.2015.1007225
12. Leng, Z., Zhang, Z., Zhang, Y., Wang, Y., Yu, H., & Ling, T. Laboratory evaluation of electromagnetic density gauges for hot-mix asphalt mixture density measurement. *Construction and Building Materials*, *158*, 1055–1064. (2018). https://doi.org/10.1016/J.CONBUILDMAT.2017.09.186
13. Meghna, & Puppanna, S. Quality Control of Hot Mix Asphalt Review. *International Journal of Applied Engineering Research I*, *13*(7), 169–173. (2018).
14. Rhee, J., Shim, J., Lee, S., & Lee, K.-H. A Consideration on the Electromagnetic Properties of Road Pavement Using Ground Penetrating Radar (GPR). *KSCE Journal of Civil and Environmental Engineering Research*, *40*(3), 285–294. (2020). https://doi.org/10.12652/KSCE.2020.40.3.0285
15. Sreedhar, S., & Coleri, E. Effects of Binder Content, Density, Gradation, and Polymer Modification on Cracking and Rutting Resistance of Asphalt Mixtures Used in Oregon. *Journal of Materials in Civil Engineering*, *30*(11), 04018298. (2018). https://doi.org/10.1061/(ASCE)MT.1943-5533.0002506
16. Teshale, E. Z., Hoegh, K., Dai, S., Giessel, R., & Turgeon, C. Ground Penetrating Radar Sensitivity to Marginal Changes in Asphalt Mixture Composition. *Journal of Testing and Evaluation*, *48*(3), 20190486. (2020). https://doi.org/10.1520/JTE20190486
17. Wang, S., Al-Qadi, I. L., & Cao, Q. Factors Impacting Monitoring Asphalt Pavement Density by Ground Penetrating Radar. *NDT & E International*, *115*, 102296. (2020). https://doi.org/10.1016/J.NDTEINT.2020.102296
18. Wang, S., Sui, X., Leng, Z., Jiang, J., & Lu, G. Asphalt pavement density measurement using non-destructive testing methods: current practices, challenges, and future vision. *Construction and Building Materials*, *344*, 128154. (2022a). https://doi.org/10.1016/J.CONBUILDMAT.2022.128154
19. Wang, S., Sui, X., Leng, Z., Jiang, J., & Lu, G. Asphalt pavement density measurement using non-destructive testing methods: current practices, challenges, and future vision. *Construction and Building Materials*, *344*, 128154. (2022b).https://doi.org/10.1016/J.CONBUILDMAT.2022.128154.
20. Wang, S., Zhao, S., & Al-Qadi, I. L. Continuous real-time monitoring of flexible pavement layer density and thickness using ground penetrating radar. *NDT & E International*, *100*, 48–54. (2018). https://doi.org/10.1016/J.NDTEINT.2018.08.005
21. Wang, S., Zhao, S., & Al-Qadi, I. L. Real-Time Monitoring of Asphalt Concrete Pavement Density during Construction using Ground Penetrating Radar: Theory to Practice. (2019).
22. *Https://Doi.Org/10.1177/0361198119841038*, *2673*(5), 329–338.

23. https://doi.org/10.1177/0361198119841038
24. Yan, Y. *Hot Mix Asphalt Concrete Density, Bulk Specific Gravity, and Permeability* [West Virginia University Libraries]. (2012).
25. https://doi.org/10.33915/etd.3348